

Mesoporous Silica Materials in Drug Delivery System: pH/Glutathione-Responsive Release of Poorly Water-Soluble Pro-drug Quercetin from Two and Three-dimensional Pore-Structure Nanoparticles

Khaled E.A. AbouAitah¹, Ahmed A. Farghali^{2*}, Anna Swiderska-Sroda³, Witold Lojkowski^{3*}, AbdelFattah M. Razin¹ and Mohamed H. Khedr²

¹Department of Medicinal and Aromatic Plants Research, Pharmaceutical and Drug Industries Research Division, National Research Centre (NRC), Dokki, Giza, Egypt

²Materials Science and Nanotechnology Department, Faculty of Postgraduate Studies for Advanced Sciences, Beni-Suef University, Beni-Suef, Egypt

³Laboratory of Nanostructures for Photonic and Nanomedicine, Institute of High Pressure Physics, Polish Academy of Sciences, Warsaw, Poland

Abstract

Quercetin (Quer) is one of natural products (pro-drugs), presenting pharmacological properties such as: anti-oxidant, anti-inflammatory and anti-cancer activities. However, poor solubility of the Quer causes its poor bioavailability, and consequently reduces its therapeutic efficiency. To manage this problem, different actions are undertaken, among other drug delivery systems (DDSs) are investigated. The objective of present work was to evaluate potential applications of silica nanoparticles as quercetin nanocarriers and to investigate the influence of pH conditions and glutathione (GSH, as non-redox process) concentrations on quercetin release.

Two types of mesoporous silica nanoparticles: MCM-41 (2D arrangement of pores) and KCC-1 (3D arrangement of pores) were synthesized and then functionalized by amino-groups. Immersion-evaporation method was used to load the Quer in nanoparticles. Several analysis techniques were used (e.g. electron microscopy, X-Ray diffraction, Zeta potential, simultaneous thermal analysis-connected to FTIR and many more). Obtained results indicated that both types of silica nanoparticles were successfully loaded with quercetin, and that the Quer present in silica mesopores had a non-crystalline structure. Loading capacity of functionalized MCM-41 was slightly higher than functionalized KCC-1 (29.11 wt% and 26.49 wt%, respectively). This difference could be attributed to the differences in the morphology structures such as surface area and pore volume property. From *in vitro* release and kinetics studies, the results showed that quercetin release from both materials was pH-GSH-silica type nanoparticles-dependent.

In summary, it can be stated that pH/GSH-stimuli release of quercetin was achieved using MCM-41 and KCC-1 amine-functionalized mesoporous silica nanoparticles as a drug carriers. Therefore both investigated nanomaterials could be beneficial for long-term release of natural pro-drug. Special attention should be paid to KCC-1 nanoparticles, as a very promising material in DDSs.

Keywords: Drug delivery system; pH and glutathione responsive release; MCM-41 and KCC-1; Mesoporous silica nanoparticles; Pro-drug of quercetin

Introduction

Based on the high-throughput screening processes, it was established that up to 40% of the new drugs are poorly-water soluble compounds [1]. Poor solubility and low dissolution rate limit significantly the biological bioavailability of drug. Therefore, poorly water-soluble drugs require special treatment to be used in the medical applications [2]. Various strategies are attempted to overcome these barriers, including: drug fragmentation to nanoscale [3], with sizing-down limitation of 20 nm [4], solid drug dispersion [5] and drug-loading into mesoporous carriers, with a special attention for nanoparticles as a drug delivery systems [6-10].

Information about mesoporous silica nanoparticles (MSNs) used in drug delivery system was published for the first time in 2001 [11]. MSNs offer many advantages, among other: simple synthesis process with pore size control in range from 2 to 50 nm, high surface area with silanol functional groups, which facilitate functionalization process, chemical and mechanical stabilities, biocompatibility and low-toxicity in the biological systems [12,13].

Mesoporous silica nanoparticles can host a various bioactive compounds and drug molecules. For instance MSNs were used to control release of the poorly water-soluble drugs such curcumin and telmisartan [4,14]. Furthermore, it was shown that solubility and dissolution rate of the drugs loaded into MSNs was enhanced

comparing to classical form of drug. This phenomenon was related to the change of drug structure from crystalline to the amorphous state [15]. It is supposed that extremely small pores size determines adequate drug refinement and that the rigid pore structure prevents re-crystallization process [16,17]. It was reported that structure of drug substance can affect the solubility of drug, where non-crystalline has more solubility comparing to crystalline state [18].

Quercetin is well known flavonoid compound, belonging to the group of natural polyphenolic compounds, ubiquitous in plants [19]. Quer presents various pharmacological effects, including anti-viral [20], anti-diabetic [21], anti-inflammatory [22] activities and protective

***Corresponding authors:** Lojkowski W, Laboratory of Nanostructures for Photonic and Nanomedicine, Institute of High Pressure Physics, Polish Academy of Sciences, Warsaw, Poland, Tel: 48602758617; E-mail: wj@unipress.waw.pl

Farghali AA, Materials Science and Nanotechnology Department, Faculty of Postgraduate Studies for Advanced Sciences, Beni-Suef University, Beni-Suef, Egypt, Tel: 002-0100-2869905; E-mail: d_farghali@yahoo.com

Received March 11, 2016; **Accepted** March 15, 2016; **Published** March 22, 2016

Citation: AbouAitah KEA, Farghali AA, Swiderska-Sroda A, Lojkowski W, Razin AM, et al. (2016) Mesoporous Silica Materials in Drug Delivery System: pH/Glutathione-Responsive Release of Poorly Water-Soluble Pro-drug Quercetin from Two and Three-dimensional Pore-Structure Nanoparticles. J Nanomed Nanotechnol 7: 360. doi:[10.4172/2157-7439.1000360](https://doi.org/10.4172/2157-7439.1000360)

Copyright: © 2016 AbouAitah KEA, et al. This is an open-access article distributed under the terms of the Creative Commons Attribution License, which permits unrestricted use, distribution, and reproduction in any medium, provided the original author and source are credited.

effect in case of neuro-inflammation [23]. Quercetin is an excellent free-radical scavenging antioxidant [24] and one of the most effective antioxidants compounds [25]. Therefore, Quer is promising substance to be used as anticancer agent [19,26]. In consequence, many *in vitro* [27] and preclinical *in vivo* [28] studies of Quer's anticancer impact have been done. It was established, that quercetin is safe in single dose up to 4 grams in oral application, and up to 100 mg in intravenous administration [29]. Such evidence opens real possibility for clinical applications of quercetin in the near future [27-30]. Despite Quer's advantages, poor biopharmaceutical characteristic, namely: poor solubility and low bioavailability and instability, limited drastically therapeutic efficiency of quercetin [31]. In this regards, a high oral dose (250 - 500 mg three times a day) is needed to be effective as a dietary supplement [32]. Going further, orally administrated Quer is extensively metabolized before reaching blood and internal organs [33]. In consequence, oral bioavailability of Quer is very poor, less than 7% of applied dose in case of rats, and less than 1% for human. Hence, application of quercetin in conventional form reduces its therapeutic effect [34]. Therefore, new approaches are needed to resolve presented obstacles. One of the directions is to use nano-carriers as a Quer delivery systems [35]. Various organic nanomaterials have been investigated, including polymeric nanoparticles and micelles, solid lipid nanoparticles, lipid nano-emulsions, PLGA nanoparticles and other. Most of these DDSs suffer from a complex preparation process and low biological stability [36]. However recently, there were published a few studies presenting interesting results obtained for MCM-41 silica nanoparticles as a DDSs for Quer [37-39]. Hence, the aim of present work was to develop and achieve pH/glutathione-responsive release of quercetin from MSNs carriers (Scheme 1). Two types of mesoporous silica nanoparticles with different morphology were examined: well-known 2D arrangement of pores (MCM-41) and 3D arrangement of pores, dendritic, fibrous with non-order pore structures (KCC-1). Both types of MSNs were synthesized and then functionalized with amino groups. The immersion-evaporation method was used to load of quercetin pro-drug. Nanoparticles were morphologically characterized at all stages of the investigations using different examination techniques, described later in the article. A few reports on quercetin release from MSNs in typical ethanol/acetate environment were published [37-39]. Our *in vitro* release tests were done using phosphate saline buffer (PBS), which adds significant values when looking for biomedical applications. It was recently reported that

glutathione can be used to trigger release from MSNs via non-redox process [40]. Hence, we tested the Quer release process under different pH conditions and various glutathione concentrations.

Materials and Methods

Materials

Cetyltrimethylammonium bromide (CTAB, Fluka), Tetraethyl orthosilicate (TEOS, 98%, Aldrich), quercetin (Sigma-Aldrich), sodium hydroxide (Sigma-Aldrich), cetylpyridinium bromide (CPB, Aldrich), cyclohexane (Sigma-Aldrich), iso-propanol (Sigma-Aldrich), acetone (Alpha Chemica, India), ethanol (Sham lab), methanol (Alpha Chemica), 3-Aminopropyltriethoxysilane (APTES 99%, Sigma-Aldrich), toluene anhydrous (POCH, Poland), dimethylsulfoxide/HPLC grade (DMSO, Tedia, USA), Urea (Sigma-Aldrich), phosphate buffer saline (PBS), and ultrapure water (18.2 MΩ, Millipore) were used for preparation of all aqueous solutions and experiments.

Synthesis of MCM-41 silica nanoparticles

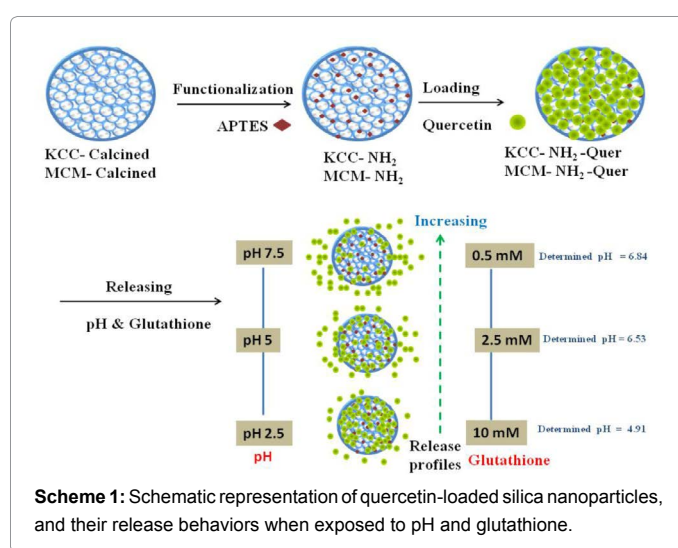
MCM-41 nanoparticles were synthesized according to previously reported method with slight modification [41]. In typical synthesis, CTAB (500 mg) was dissolved in ultrapure water (240 ml) with 2M of sodium hydroxide solution (1.750 ml) under vigorous stirring for 1 h. Then, the mixture was heated up to 85°C, and after temperature stabilization 2.5 ml of TEOS was slowly dropwise added. TEOS was allowed to hydrolyze for 2 h. After completion of the chemical reaction, the solution was cooled down to room temperature. Silica nanoparticles were collected by centrifugation and then washed several times with absolute methanol, and dried in ambient atmosphere for 12 h. To remove the template surfactant molecules from the mesopores, as-synthesized material was calcined at 600°C for six hours in air. The resulting material was named MCM-Calcined.

Synthesis of KCC-1 silica nanoparticles

The three dimensional mesoporous silica nanoparticles with fibrous and dendritic pore networks were prepared for the first time with hydrothermal method [42]. This procedure was modified to produce KCC-1 silica nano-spheres without hydrothermal assistance method [43]. In present work we prepared KCC-1 nanoparticles with some modifications. In a typical synthesis, 1 g of cetylpyridinium bromide and 0.6 g of urea were dissolved in 30 ml of ultrapure Millipore 18.2 MΩ under stirring for 30 min. Subsequently, 30 ml of cyclohexane and 1.2 ml of iso-propanol were added to the solution. With vigorous stirring, 2.7 ml of TEOS was slowly dropwise added to the mixed solution. After 30 min of vigorous stirring at room temperature, the mixture was heated up to 85°C, and this condition was maintained for 17 h. In order to collect the silica nanoparticles, liquid suspension was centrifuged. Nanoparticles were washed several times with acetone and water, and then dried for 12 h at room temperature. To remove the surfactant template from the surface of prepared silica, as-synthesized material was calcined at 600°C for six hours in air. The resulting material was named as KCC-Calcined.

Post-synthesis functionalization of mesoporous silica materials with amines groups

The amine-functionalization was performed by reacting the KCC-Calcined or MCM-Calcined with anhydrous toluene, according to previous report [44] with slight modifications. To graft aminopropyl groups on the mesopore's surface of MSNs, before functionalization, samples were dried at 50°C for 5 h, to remove the physically adsorbed



Scheme 1: Schematic representation of quercetin-loaded silica nanoparticles, and their release behaviors when exposed to pH and glutathione.

water. Typically, anhydrous toluene (100 ml) and KCC-Calcined or MCM-Calcined (1 g) were first dispersed via sonication for 30 min., then 1.5 ml of APTES was added under stirring and the mixture was stirred at room temperature for 24 h. The solid products were isolated after cooling the mixture solution at room temperature by centrifugation. Functionalized nanoparticles were washed with ethanol three times and then dried for 12 h in ambient atmosphere. Finally, samples were heated at 50°C during 12 h in air. The 3-aminopropyl-grafted materials were named as MCM-NH₂ and KCC-NH₂.

Drug loading

In present study, the Quer loading process was carried out according to solvent evaporation method [45] with some modifications. The solvent of mixture from ethanol/DMSO/acetone (1:1:5, respectively) was used in the procedure. Drug loading process involved two steps: initial loading/adsorption and evaporation of solvent.

Then 300 mg of MCM-NH₂ or KCC-NH₂ were added to solvent containing 100 mg of Quer, to obtain mass ratios of drug to silica equal to 1:3. Suspensions were stirred for 12 h at room temperature (first step). After that, the samples were evaporated at 50°C using the Rotavap (Büchi, Switzerland) with the water bath set (second step). Finally, nanoparticles were re-dispersed in water in order to remove unloaded quercetin molecules. The Quer-loaded silica nanoparticles were collected by centrifugation, and then washed several times with water. Finally, the samples were dried at 40°C for 12 h. The resulting materials were denoted MCM-NH₂-Quer and KCC-NH₂-Quer.

In vitro release studies

In vitro release tests were done in phosphate saline buffer (PBS) during 100 h. Typically, 25 mg of MCM-NH₂-Quer or KCC-NH₂-Quer were dispersed in 35 ml of PBS buffer solution adjusted to different pH values (2.5, 5 and 7.5). In case of glutathione experiments, GSH amounts equal to three concentrations of 0.5, 2.5 and 10 mM were added to the PBS release media. The solutions were stirred at 37°C for 100 h. At predetermined intervals of times, 1.5 ml aliquots were taken to detect present Quer concentration (cumulative release). The aliquots were centrifuged to eliminate silica nanoparticles from solution. Liquid samples (after centrifugation) were analyzed using UV-Vis spectroscopy at $\lambda = 375$ nm. The experiments were conducted in duplicate, and obtained results were averaged. Usually, in order to maintain a constant volume of the release medium during the entire period of release tests, each time after sampling for analysis (e.g. UV-Vis), adequate volume of fresh medium (without drug-loaded material) is added. In such procedure an equation is needed to calculate the release profiles. But in our experiments we conducted release tests in two containers at the same time for each sample as described above and after each sampling for analysis, we was added similar volume (sampling volume for analysis) from one container to another container, thus the volume was constant with the real sample and thus this lead to avoid using an equation if we use fresh medium.. Then, amount of Quer released from nanoparticles was calculated according to the simple equation:

$$\text{Cumulative release (\%)} = (\text{Amount of Quer released to solution}/\text{Amount of Quer placed in MSNs}) \times 100\%.$$

Characterization techniques

The HR-TEM images were taken using High Resolution Transmission Electron Microscope JEOL, JEM 2100, Japan. The morphology and chemical compositions of the samples were also

performed on the Field Emission Scanning Electron Microscope (Zeiss Ultra Plus, Germany) equipped with QUANTAX EDS, Bruker. Different preparation techniques of the samples were used. Samples were sputter with carbon or gold-palladium via a sputter coater (Bal-Tech SCD 005), and chromium via a (Quorum, Q150T ES) prior to imaging. X-ray diffraction (XRD) patterns were recorded (PANalytical, X'Pert PRO System) using CuK α radiation in the 2 θ range of 10-100°. Nitrogen adsorption-desorption isotherms were measured using a Quantachrome NOVA Automated Gas Sorption System. Before measurements, samples loaded with drugs were degassed at 50°C for 24 h., while the samples without drugs were degassed at 120°C for 12 h. The specific surface areas were measured based on the BET (Brunauer-Emmett-Teller) method. The pore size distributions were obtained from the adsorption/desorption branches of the isotherms, based on the density functional theory (DFT). The total pore volumes were calculated from the adsorption data at the maximum relative pressure (P/P₀). To evaluate the loading percent and efficiency, the samples were examined using thermal gravimetric analysis (TGA-50, Shimadzu, Japan). TGA was performed with a heating rate of 10°C/min in continuous air flow. To determine functional groups and chemical bonding, the powder samples were characterized using Fourier transformed infrared (FTIR) spectroscopy (Bruker, Tensor 27) equipped with a Attenuated Total Reflectance (ATR, model Platinium ATR-Einheit A 255). For each ATR-FTIR spectra 100 scans were collected, in the ranges of 350-4000 cm⁻¹. Simultaneous Thermal Analysis (STA) collecting in the same time thermogravimetry (TG) and Differential Scanning Calorimetry (DSC) data were performed using STA 499 F1, Jupiter, Netzsch. Samples weighting ca. 10-20 mg were loaded into alumina pan of the STA unit, and before measurements, the helium flow through the STA furnace chamber was applied during 30 min. The experimental parameters were programmed to reach 700°C with a heating rate of 10°C/min under a helium purge of 60 ml/min. Gasses evolved during thermal experiments were analyzed *in situ*, thanks to coupling of the STA instrument with FTIR spectrometer. Zeta potential measurements for water suspension of nanoparticles (concentration of 1 mg/ml) were performed at 24°C using a Malvern ZetaSizer (NanoZS).

Results and Discussions

Structural and morphological characterization

The structural and morphological features of the calcined materials are shown in Figure 1. SEM observations of the KCC-Calcined silica

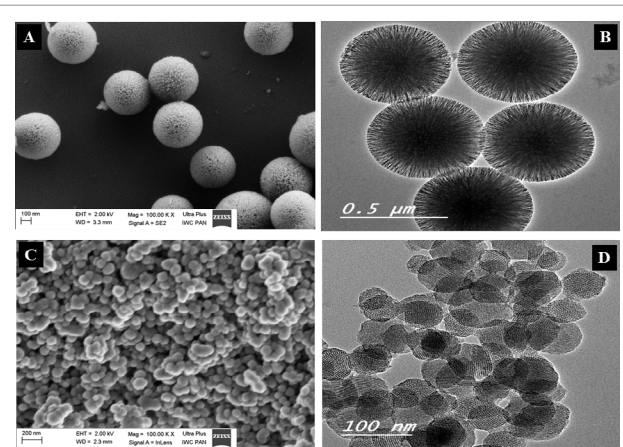


Figure 1: SEM and TEM images of mesoporous silica nanoparticles: KCC-Calcined (A and B) and MCM-Calcined (C and D).

(Figure 1A) showed that the sample consisted of non-aggregated, monodisperse spherical particles, ranging from 200 to 500 nm in diameter, formed by dendrimeric fibers. This observation is similar to SEM images from previous studies related to this material [42,43]. TEM images of KCC-Calcined established well dispersion and narrow size distribution of the nanoparticles. In particular, particles possessed an interesting fibrous dendritic structure with fibers coming out from the centre and distributed uniformly in all directions (Figure 1B), which is also consistent with the mentioned publications [42,43]. In case of MCM-Calcined, the sample consisted of roughly spherical nanoparticles ranging from 100 nm to 170 nm in diameter, with some aggregation tendency, and exhibited hexagonally ordered cylindrical pores (Figures 1C and 1D).

To determine the chemical composition of MSNs, the Energy-dispersive X-ray spectroscopy (EDS) analysis was utilized. Results are presented in Supporting Information, Figures SI1 and SI2. MCM-Calcined and KCC-Calcined nanoparticles composed of silicon and oxygen, which confirmed formation of the silica during the synthesis process (Figure SI1). While, amine-functionalized samples: MCM-NH₂ and KCC-NH₂ composed of silicon, oxygen and nitrogen (Figure SI2), which verified functionalization of the nanoparticles. The same elements were detected for KCC-NH₂-Quer and MCM-NH₂-Quer.

Drug loading and characterization

N₂ adsorption/desorption analysis

Nitrogen adsorption/desorption analysis of nanoparticles were done at all stages of the MSNs investigations. Results obtained for non-modified, modified and Quer-loaded materials are presented in Table 1 and Figure 2. The MCM-Calcined and KCC-Calcined have isotherms type-IV (according to the IUPAC classification), typical for mesoporous structures (Figure 2A-2D). It was observed that from pore size distributions of MCM-Calcined particles, this material exhibited narrow pore size distributions, where a single sharp peak (at about 2 nm) with another lower intensity peak (at about 2.6 nm) were observed (Figure 2A and 2B). KCC-Calcined nanoparticles presented much wider pore size distributions (main peak was observed about 3.4 nm), which indicated non-uniform porous structure (Figure 2C and 2D). It can be attributed to the unique pore system with 3D arrangement of dendritic mesopore form [42]. As shown in Table 1, MCM-Calcined and KCC-Calcined differed also in average of pore size diameters, reaching 2.43 nm and 3.36 nm, respectively. Regarding BET analysis, MCM-Calcined nanoparticles showed a higher specific surface area (963 m²/g) compared to KCC-Calcined (585 m²/g). After the functionalization with amino groups, the pore size distributions and surface area were

decreased, suggesting that the presence of aminopropyl groups in both materials and successful functionalization process.

Adsorption/desorption isotherms and pore size distributions of MCM-NH₂-Quer and KCC-NH₂-Quer varied in comparison to the curves obtained for calcined and modified materials (Figure 2). Nature of the registered changes suggests presence of the pro-drug inside silica mesopores. This assumption was confirmed by drastic reduction of the: specific surface area, total pore volume and average pore size of loaded-materials. Similar effects of nano-Quer aggregated into the pores of nanoparticles was also described by [46]. Presented results are in line with the XRD and DSC data and in good agreement with reports published previously [10,47,48].

Determination of drug loading efficiency by TGA analysis

Quantitative analysis of functional groups and quercetin entered to the structure of the MSNs were done using TGA method. Results are presented in Figure 3 and Table 1. Experiments showed, that amounts of aminopropyl groups attached to the surface of MCM-NH₂ was lower than in case of KCC-NH₂ silica and reached 5.49 wt.% and 8.92 wt.%, respectively. However, quercetin content in MCM-NH₂-Quer (29.11 wt.%) was higher compared to KCC-NH₂-Quer (26.49 wt.); the loading efficiency was 87.41% and 79.54% in MCM-NH₂-Quer and KCC-NH₂-Quer, respectively. The slightly higher drug loading

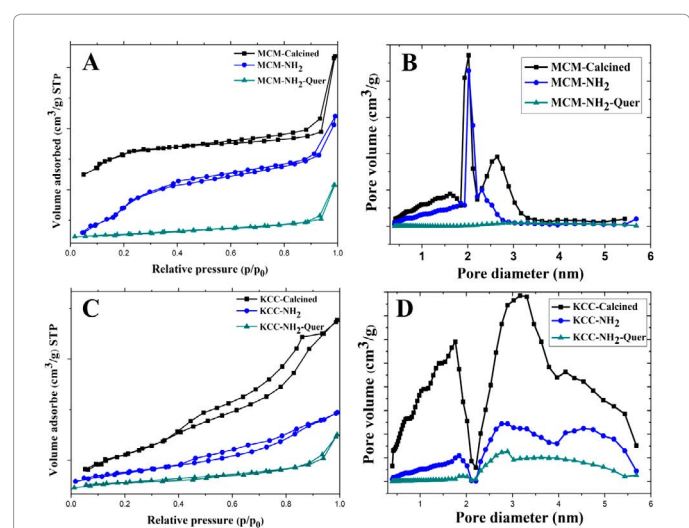


Figure 2: Nitrogen adsorption/desorption isotherms and pore size distributions of MSNs: MCM-Calcined, functionalized and Quer-loaded (A) and KCC-Calcined, functionalized and Quer-loaded (B).

Sample	S _{BET} (m ² /g)	Pore Volume ^a (cm ³ /g)	Pore Size ^b (nm)	Amount of aminopropyl groups ^c (wt.%)	Nitrogen Content ^d (wt.%)	Quer Content ^e (wt.%)	Quer Loading Efficiency ^f (wt.%)
MCM-Calcined	963	0.868	2.43	-	-	-	-
KCC-Calcined	585	0.91	3.36	-	-	-	-
MCM-NH ₂	500	0.75	1.87	5.49	2.91	-	-
KCC-NH ₂	172	0.385	2.88	8.92	3.42	-	-
MCM-NH ₂ -Quer	71	0.292	1.38	-	2.68	29.11	87.41
KCC-NH ₂ -Quer	77	0.493	2.62	-	3.06	26.49	79.54

^a Pore volume obtained from DFT theory method

^b Pore size calculated by DFT theory method.

^c Calculated from TGA analysis.

^d Obtained from EDS analysis

^e and ^fCalculated from TGA analysis.

Table 1: Physicochemical properties of the calcined, functionalized and quercetin-loaded materials.

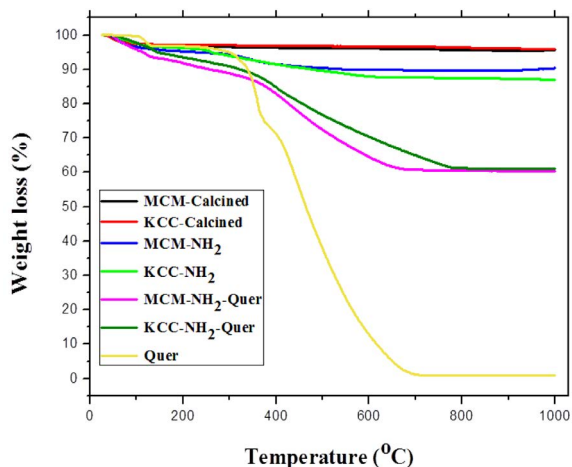


Figure 3: TG profiles of calcined, amine-functionalized and quer-loaded MSNs.

content in MCM-NH₂ compared to KCC-NH₂ could be attributed to surface area and pore volume property instead of pore size of property as listed in Table 1. Our results confirm earlier statement, that the morphological parameters such as: surface area and pore volume, pore size, influence significantly drug loading efficiency [13]. Presented results are also in accordance with previous studies [49].

Characterization of MSNs by XRD and DSC techniques

As was described earlier, crystalline state of pro-drug influences its solubility and release efficiency. Therefore, we examined crystal structure of pure Quer and Quer mixed with nanoparticles, as a reference materials, and Quer-loaded MSNs. Two complementary techniques were used: XRD and DSC. Results are presented in Figures 4 and 5, respectively.

Diffraction patterns of pure quercetin presented peaks at: 10.59°, 12.54°, 13.65°, 24° and 27.51°. Similar pattern was obtained for physical mixtures of Quer and MSNs, with peaks at 10.59°, 12.54° and 27.51. On the other side, MCM-NH₂-Quer and KCC-NH₂-Quer samples did not show any diffraction peak corresponding to pure quercetin. This might be attributed to Quer molecules were transformed to non-crystalline form. This is consistent with the results of previous studies [10,18,48].

DSC curve of pure Quer presented a single endothermic melting peak at 328°C, characteristic for crystalline quercetin. Whereas, DSC curves registered for MCM-Calcined, KCC-Calcined, MCM-NH₂, KCC-NH₂, MCM-NH₂-Quer and KCC-NH₂-Quer were similar each other and did not show peaks at the Quer melting temperature. Thus, DSC analysis of drug-loaded MSNs confirmed XRD results and provided evidence that Quer was transformed to a non-crystalline structure. Hence, from the XRD and DSC examination, we conclude that the Quer was successfully loaded into mesoporous silica nanoparticles in non-crystalline form. Our achievement is with accordance with data obtained by other researchers [49-51].

FTIR spectroscopy analysis

Organic functionalization and drug loading were evidenced from FT-IR spectra; all of the prepared materials (MCM-Calcined, KCC-Calcined, MCM-NH₂, KCC-NH₂, MCM-NH₂-Quer and KCC-NH₂-Quer) showed the siliceous framework in FTIR spectra (Figure S13 in supporting information). The FT-IR spectra of MCM-Calcined and

KCC-Calcined samples were characterized by appearance of several bands related to the siliceous framework: A broad band observed at about 1070 cm⁻¹ attributed to the asymmetric stretching vibration of Si-O-Si. While, two bands presented at 810 cm⁻¹ and 450 cm⁻¹ corresponded to the symmetric stretching vibration of Si-O-Si and the bending vibration of Si-O-Si, respectively [52-54]. In addition, absence of bands typical for alkyl C-H stretching frequencies at 2850 cm⁻¹ and 2922 cm⁻¹ after calcination, confirmed removal of the surfactant templates from the prepared materials [55].

For the functionalized-materials with aminopropyl groups using APTES, new bands were observed in the region between 1350 cm⁻¹ to 1700 cm⁻¹ (Figure 6A): two bands observed at 1390 cm⁻¹ and 1450 cm⁻¹ attributed to the presence of ethoxy groups [56], a band at 1495 cm⁻¹ might be attributed to C-H asymmetric and symmetric stretching vibrations [57], a band observed at 1556 cm⁻¹ corresponded to -NH₂ asymmetric bending and C-H stretching vibrations [14,58], and a band about at 1650 cm⁻¹ might be attributed to asymmetric deformation of protonated amine groups -NH₃⁺ [59,60]. Together with additional band observed at 2939 cm⁻¹ (Figure 6B) associated to C-H as a result of

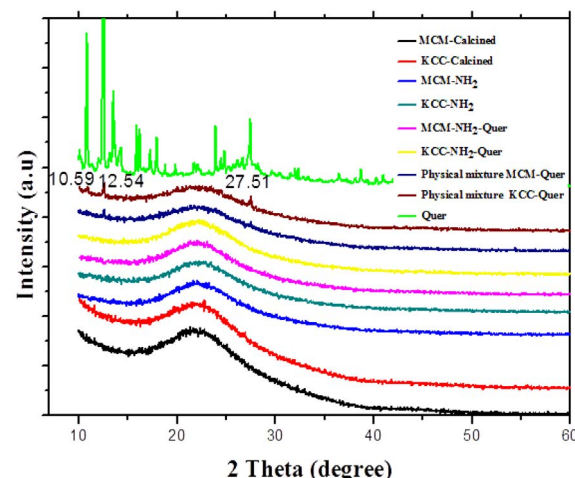


Figure 4: XRD patterns of MSNs at different research stages: MCM-Calcined, KCC-Calcined, MCM-NH₂, KCC-NH₂, MCM-NH₂-Quer and KCC-NH₂-Quer.

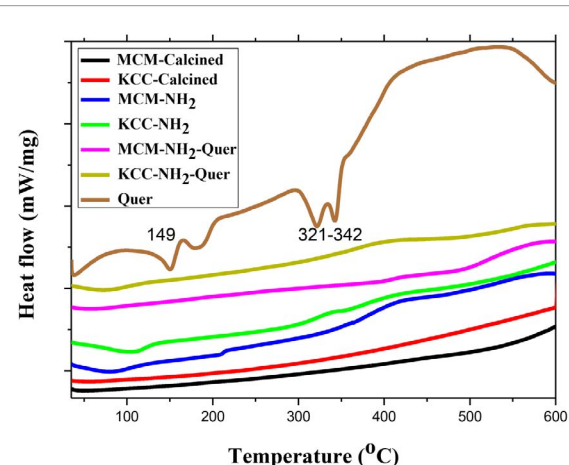


Figure 5: DSC profiles of Quercetin and MSNs at different research stages: MCM-calcined, KCC-calcined, MCM-NH₂, KCC-NNH₂, MCM-NH₂-Quer and KCC-NH₂-Quer.

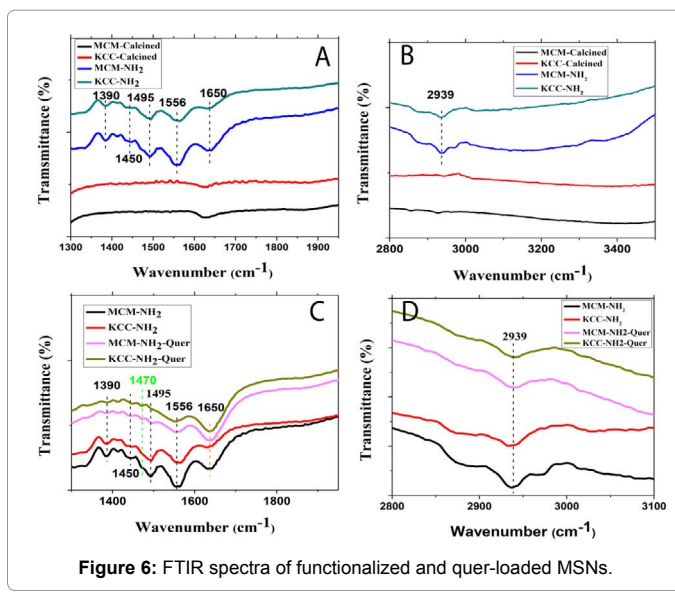


Figure 6: FTIR spectra of functionalized and quer-loaded MSNs.

introducing the methyl groups and propyl chain during silylation [58]. Moreover, a band observed at 960 cm^{-1} which attributed to vibrational band of silanol groups Si-OH was showed some alterations after the functionalization process, as result of consumption of silanol groups during the interaction of APTES molecules with surface of silica nanoparticles [61] (Figure S13 supporting information). FTIR spectra of modified MSNs proved efficiency of the functionalization process.

For quercetin-loaded materials (MCM-NH₂-Quer and KCC-NH₂-Quer) (Figure 6), a new band observed at 1470 cm^{-1} , might be attributed to a slight shift from 1445 cm^{-1} in pure quercetin band (supporting information). It was noted that the all bands observed after functionalization at 1390 , 1450 , 1495 and 1556 cm^{-1} were strongly decreased, suggesting that both of N-H and NH₃₊ amino groups associate in the interaction with quercetin molecules; while, a band at 1650 cm^{-1} slightly increased after quercetin loading (Figure 6C). In addition, a band observed at 2939 cm^{-1} decreased as compared to similar band after functionalization with amino groups (Figure 6D). Taken all together, FTIR spectra could be confirmed that the quercetin loaded into silica framework was in non-crystalline state.

Zeta potential measurements

Since, the surface charges of MSMs play important roles to be internalized by cells and escape endosomal entrapment [62], and the loading and sustained release [63]. We measured the zeta potential of all prepared materials suspended in an aqueous media, with various pH levels from 2 to 12. As shown in Figure 7, zeta potential/pH curves of calcined nanoparticles showed very small values of positive charges (around +2 to +3) between pH 2 to 2.5. By further increasing the pH up to 12, the calcined nanoparticles exhibited negative charge values. For instances, at neutral pH 7, the values were about -35 and -46 for MCM-calced and KCC-Calced, respectively. While, at pH 12, the obtained values were about -33 and -55 for MCM-calced and KCC-Calced, respectively. These probably due to the silanol groups distribute on silica surface were deprotonated, leading to cause negative zeta potential values [63,64].

After functionalization with amino-groups using APTES, MCM-NH₂ and KCC-NH₂ showed higher positive charged values; the maximum positive charges recorded at pH 2.5 was to be +38.5 and +55 in MCM-NH₂ and KCC-NH₂, respectively. With increasing the pH

to 7, the obtained values were about +20 and +37 for MCM-NH₂ and KCC-NH₂, respectively. Thus, functionalized nanoparticles still possess positive charges compared to calcined nanoparticles, which possess negative charges on their surfaces. By further increasing pH to 12, functionalized nanoparticles exhibited negative charges about -52 and -48 for MCM-NH₂ and KCC-NH₂, respectively. This well proves the successful functionalization with amino groups on the surface. These results agreed with previous reported studies [65,66].

Further, loading of the quercetin to amine-functionalized silica nanoparticles (MCM-NH₂-Quer and KCC-NH₂-Quer), leads to decrease zeta potential values under pH from 2 to 12 compared to functionalized and calcined nanoparticles, respectively. Where, the quercetin-loaded nanoparticles showed lower zeta values corresponding to functionalized nanoparticles and higher values compared to calcined nanoparticles. The zeta-potential variations well indicate the successful loading of quercetin to amine-functionalized silica nanoparticles.

Qualitative analysis of the evolved gasses by STA-FTIR techniques

Simultaneous Thermal Analysis (STA) coupled with Fourier Transform Infrared spectroscopy (STA-FTIR), it is a powerful tool to qualitative analysis of the gases involved during desorption or pyrolysis process [67,68].

All types of samples were investigated using FTIR spectrometry coupled with STA apparatus. FTIR absorption three-dimensional spectra as a function of wave number and temperature were registered (Figure S14, supporting information). However, particular FTIR absorbance spectra can be identified for selected temperature (reddish brown line) to show the gases released at specific condition, in accordance with TG results. For MCM-Calced and KCC-Calced samples weight loss was observed at 220°C on TG curves. As it can be seen in Figure S3A and S3B, this mass fall corresponds to FTIR signals of: O-H stretch for water with a weak intensity band (3600 and 3850 cm^{-1}), CO₂ (2200 and 2400 cm^{-1}), and H₂O (1300 and 1700 cm^{-1}).

In case of MCM-NH₂ and KCC-NH₂ samples (Figure S14) desorption of physically adsorbed water molecules was detected during the first mass loss below 100°C , while decomposition of aminopropyl groups between 150 - 400°C [69,70]. Mass loss observed at temperature about 450°C was associated with: O-H for water, CO₂, H₂O, and

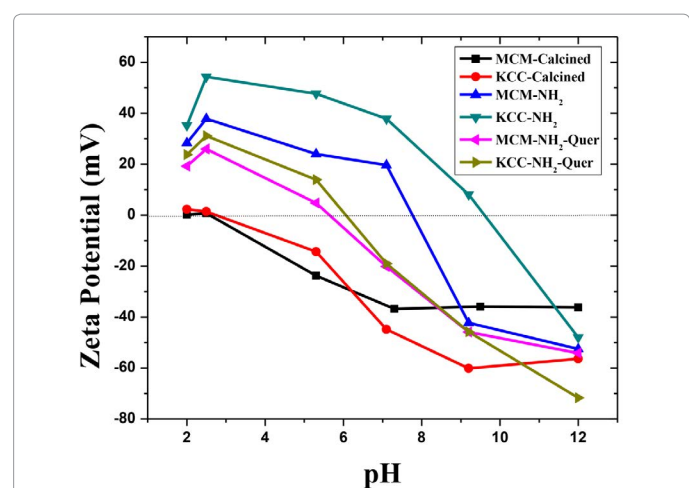


Figure 7: Zeta potential measurements of MSNs in initial state, functionalized and Quer-loaded.

CH₄ (a band around 400 cm⁻¹). It was observed that the band at 2200 cm⁻¹ which related to CO₂ exhibited higher absorbance intensity at temperature about 450°C in both functionalized materials with similar intensity. This observation could be confirms that the presence of organic aminopropyl molecules. By further quercetin loading to functionalized nanoparticles, the CO₂ band showed higher intensities about 0.25 (MCM-NH₂-Quer) and 0.35 (KCC-NH₂-Quer) compared to MCM-NH₂ (0.12) and KCC-NH₂ (0.10) Figure SI4E and SI4F). This finding could be further confirms the successful loading of quercetin. By investigating the pure quercetin compound, it was found that CO₂ band indicated higher intensity than that of Quer-loaded nanoparticles, which about 1.5 (Figure SI4). These differences suggest that STA-FTIR could be useful technique for such studies.

In vitro release and drug kinetic studies

In vitro release

Quer release profiles were first investigated with different pH values of phosphate saline buffer media (PBS) (low, mildly and neutral pH values: 2.5, 5 and 7.5, respectively). The release profiles were also investigated under different glutathione concentrations (0.5, 2.5 and 10 mM). The cumulative release profiles of MCM-NH₂-Quer and KCC-NH₂-Quer are presented in Figure 8. Generally, quercetin was released gradually during whole experiment (100 hours), with the nearly linear release profile. However, release behaviors of quercetin from both silica materials were pH/glutathione-dependent. Release of Quer from both materials was significantly more intense in neutral pH condition, than that of low and mildly acidic conditions. On the other hand, Quer release increased with decreasing of the GSH concentration.

For MCM-NH₂-Quer material, release profiles under different pH conditions and glutathione concentrations are presented in Figure 8A.

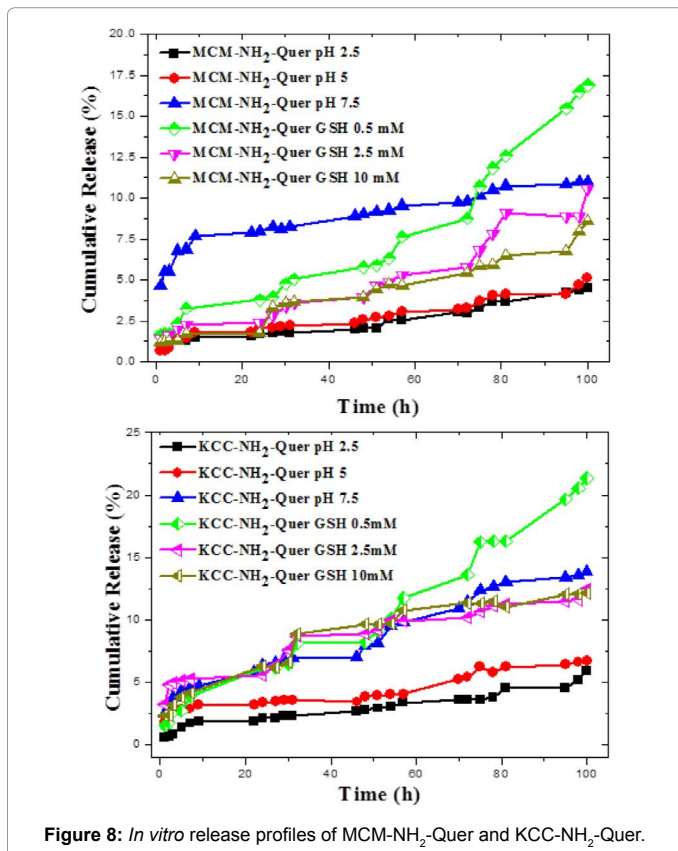


Figure 8: *In vitro* release profiles of MCM-NH₂-Quer and KCC-NH₂-Quer.

It can be seen that Quer release reached 11%, 5.1% and 4.5%, for pH levels: 7.5, 5 and 2.5, respectively. Regarding to GSH influence, it was noted that release reached 16.89%, 10.57% and 8.59% for glutathione concentration: 0.5 mM, 2.5 mM and 10 mM, respectively. In case of KCC-NH₂-Quer material, similar tendency as for MCM-NH₂-Quer was observed, however amount of released Quer was higher (Figure 8B). The release was greatest for neural condition (pH 7.5) and reached 13.88%, in mildly acidic condition (pH 5) it was 6.7%, and for low acidic condition (pH 2.5) reached 5.89%. Experiments conducted in function of glutathione concentration showed following cumulative releases: 21.34% for glutathione concentration of 0.5 mM, 12.47% for 2.5 mM and 6.7% for highest GSH concentration 10 mM. Based on glutathione results, it was observed that glutathione played an important role in modulation of Quer release from silica carriers. Unlike the extensively studied redox-trigger release systems via disulfide bonds; it was reported that release is connected with a non-redox and ionic processes associated with glutathione and glutathione-induced pH changes [40]. To distinguish release of Quer from both materials is related to glutathione effect or glutathione-induced pH changes, in our work the pH values of: 6.84, 6.53 and 4.91 were recorded for following glutathione solutions: 0.5 mM, 2.5 mM and 10 mM, respectively. It was noted that, the release profiles observed with GSH 10 mM (pH 4.91, which close to 5) were not similar to those obtained at pH 5 without GSH. This observation suggesting that the differences in release profiles related to influence of glutathione other than glutathione-induced pH changes.

Obtained results show that the quercetin was not completely transferred from MSNs to PBS medium and that the Quer release efficiency can be controlled by the pH or glutathione concentrations. This finding is consistent with results obtained for curcumin (poorly water-soluble pro-drug) loaded into MCM-NH₂ material, where the maximum release reached 22.23%, in 0.5% sodium lauryl sulphate medium [50]. Maximum cumulative release of quercetin was higher for KCC-NH₂-Quer (21.34%) than for MCM-NH₂-Quer (16.89%). This can be attributed to the differences in nano-carriers morphologies. KCC-Calcined presented larger pore size and wider pore size distribution, fibrous structure with dendrimeric mesopores arranged in 3D. Thus, the Quer release took place gradually with different rates over time. MCM-41 had much smaller pore size and narrower pore-size distribution compared to KCC-1. Such pore structure leads to hinder, and consequently reduces release of the quercetin to the liquid medium [67-72]. Our results are in agreement with work reporting more intense drug release from 3D mesopores arranged structures than from 2D type [48]. It was also shown that pore size affected drug diffusion: the smaller mesopores, the smaller release kinetic constant [13]. Therefore our work showed that KCC-NH₂ silica nanoparticles are more promising as Quer carriers than MCM-NH₂ modified silica.

As the functionalization plays important role in release of drugs, for instance, the functionalized-MSNs with aminopropyl groups using APTES are able to regulate drug release. APTES reduces influx of liquid media in the pores and then eventually delay the release of drug. This phenomenon may impart relatively slight hydrophobicity [50]. As well as, APTES would impart some stearic hindrance inhibiting the drug release from MSNs [73]. Thus, the amino-groups in MCM-NH₂ and KCC-NH₂ contribute to delay of quercetin release. Our results also agree with previous reported study [74].

Drug kinetic studies

To analyze the *in vitro* release profiles data, several kinetic models can be used. In some studies, the Higuchi model was used [75-77], in other cases, the first-order kinetic exponential decay model was

employed [53,75,78], the Korsmeyer-Peppas model was used [79-81], or the Zero-order model with other models were utilized [82]. In our study, kinetic models for quercetin kinetic release studies were chosen: Zero-order, Higashi and Kmeyer-Peppas models was used to describe the kinetic release; the later model was employed mainly to describe the release mechanism of quercetin from nanoparticles. The obtained cumulative% release data of Quer under pH conditions and glutathione concentrations were fitted in all models, the estimation was performed with the DDSolver software [83]. The parameters of K₀ (zero-order release constant), K_H (Higashi model release constant) and R² (coefficient of determination) obtained after fitting the Quer release data with models are listed in Table 2. It can be seen that, the kinetic release of Quer from two materials depends on the responsive release stimuli factor (pH and GSH) and nanoparticles type. Generally, the R² values obtained for MCM-NH₂-Quer and KCC-NH₂-Quer under pH conditions was closed to or higher than 0.900 (except the KCC-NH₂-Quer and MCM-NH₂-Quer under pH conditions 5 and 7.5, respectively, showed lower values), when fitted to Higushi model. The recorded R² values were 0.900, 0.907, 0.917, 0.803, 0.704 and 0.930 for MCM-NH₂-Quer (pH 2.5), KCC-NH₂-Quer (pH 2.5), MCM-NH₂-Quer (pH 5), KCC-NH₂-Quer (pH 5), MCM-NH₂-Quer (pH 7.5) and KCC-NH₂-Quer (pH 7.5), respectively. These results indicated that, most of Quer release from materials under pH factor fit to Higushi model. Moreover, the K_H values increased with increasing the pH level: they were 0.395, 0.459, 0.428, 0.664, 1.278 and 1.337 for MCM-NH₂-Quer (pH 2.5), KCC-NH₂-Quer (pH 2.5), MCM-NH₂-Quer (pH 5), KCC-NH₂-Quer (pH 5), MCM-NH₂-Quer (pH 7.5) and KCC-NH₂-Quer (pH 7.5), respectively. The increase of K_H values with increase of pH demonstrate that for higher pH level Quer release rate is increasing. On the other hand, when the Zero-order model was applied to these materials, this model did not allow for a good fit, since the R² values not reach 0.90 and R² was up to 0.767 at all.

For release of Quer from silica nanoparticles under GSH concentrations, it can be seen that, in general trend, the R² values obtained for MCM-NH₂-Quer and KCC-NH₂-Quer under various GSH concentrations was to or higher than 0.900 (except the KCC-NH₂-Quer with GSH concentration of 2.5 mM and 10 mM, showed lower values) when fitted to zero-order model. The recorded R² values were 0.925, 0.963, 0.910, -0.365, 0.921 and 0.540 for MCM-NH₂-Quer (GSH: 0.5 mM), KCC-NH₂-Quer (GSH: 0.5 mM), MCM-NH₂-Quer (GSH: 2.5 mM), KCC-NH₂-Quer (GSH: 2.5 mM), MCM-NH₂-Quer (GSH: 10 mM) and KCC-NH₂-Quer (GSH: 10 mM), respectively.

The obtained results demonstrated that, most of Quer release from materials under GSH factor fit to zero-order model. In this context, the K₀ values decreased with increasing the GSH concentration: they were 0.151, 0.206, 0.097, 0.146, 0.081 and 0.136 for MCM-NH₂-Quer (GSH: 0.5 mM), KCC-NH₂-Quer (GSH: 0.5 mM), MCM-NH₂-Quer (GSH: 2.5 mM), KCC-NH₂-Quer (GSH: 2.5 mM), MCM-NH₂-Quer (GSH: 10 mM) and KCC-NH₂-Quer (GSH: 10 mM), respectively. Thus decrease of K_H values with increase of GSH concentration indicated that for higher GSH level Quer release rate is decreasing. On the other side, when the Higushi model was applied to these materials, this model did not allow for a good fit for the most of samples except the KCC-NH₂-Quer sample under 2.5 M and 10 mM, since the R² values were: 0.786, 0.873, 0.883, 0.925, 0.880 and 0.956 for MCM-NH₂-Quer (GSH: 0.5 mM), KCC-NH₂-Quer (GSH: 0.5 mM), MCM-NH₂-Quer (GSH: 2.5 mM), KCC-NH₂-Quer (GSH: 2.5 mM), MCM-NH₂-Quer (GSH: 10 mM) and KCC-NH₂-Quer (GSH: 10 mM), respectively. This observation indicates that silica type of nanoparticles is another factor can be influenced the kinetic release of Quer together with pH and GSH; where under GSH experiments, the KCC-NH₂-Quer exposed to GSH (10 mM) was showed good fit to Higushi model, while under same GSH condition, MCM-NH₂-Quer showed good fit to zero-order model. These results confirm that the quercetin release kinetics is dependent on stimuli release factor (pH and GSH) and type of silica nanoparticles. It was reported that morphology structure of nanocarriers determine the interface between drug-loaded systems and the release medium, leading to influence the drug release kinetics [54,71,84,85].

For understanding drug release mechanism of our delivery system, the Korsmeyer-Peppas model [86] was employed (see equation 1).

$$Mt / M_{\infty} = kt^n \quad (1)$$

Where Mt and M_∞ denote the cumulative mass of drug released at time t and at infinite time, respectively; K is a kinetic constant characteristic of the drug-carrier system; and n is an exponent (release index), which is indicative of the mechanism of the drug release. The release index n gives the information about the release mechanism of drug: n ≤ 0.45, represents a Fickian Diffusion [87]. If n > 0.45 and < 0.89, a non-Fickian or anomalous diffusion is present; n = 0.89, provides a case II transport, while n > 0.89, indicates a zero-order mechanism [88].

The release data were fitted to this model from both materials under different pH conditions and GSH concentrations and listed in

Material	Responsive condition	Zero order		Higuchi	
		pH	K ₀ (% h ⁻¹)	R ²	K _H (% h ⁻¹)
MCM-NH ₂ -Quer		2.5	0.143	0.411	0.395
KCC-NH ₂ -Quer		2.5	0.055	0.767	0.459
MCM-NH ₂ -Quer	GSH	5	0.051	0.738	0.428
KCC-NH ₂ -Quer	GSH	5	0.076	0.202	0.664
MCM-NH ₂ -Quer	GSH	7.5	0.144	0.331	1.278
KCC-NH ₂ -Quer	GSH	7.5	0.151	0.669	1.337
MCM-NH ₂ -Quer		0.5 mM	0.151	0.925	1.244
KCC-NH ₂ -Quer		0.5 mM	0.206	0.963	1.71
MCM-NH ₂ -Quer		2.5 mM	0.097	0.91	0.806
KCC-NH ₂ -Quer		2.5 mM	0.146	0.365	1.248
MCM-NH ₂ -Quer		10 mM	0.081	0.921	0.687
KCC-NH ₂ -Quer		10 mM	0.13	0.544	1.299

R²: correlation coefficient, K₀: zero-order rate constant, K_H: Higuchi rate constant.

Table 2: Kinetic parameters of quercetin release from silica materials as drug carrier systems under different pH conditions based on mathematical models.

Material	Responsive condition	Korsmeyer-Peppas model			Mechanism	
		pH	K(h^{-n})	R ²		
MCM-NH ₂ -Quer		2.5	0.293	0.909	0.572	non-Fickian or anomalous diffusion
KCC-NH ₂ -Quer		2.5	0.377	0.910	0.548	non-Fickian or anomalous diffusion
MCM-NH ₂ -Quer		5	0.394	0.918	0.520	non-Fickian or anomalous diffusion
KCC-NH ₂ -Quer		5	1.246	0.906	0.340	Fickian diffusion
MCM-NH ₂ -Quer		7.5	3.330	0.958	0.243	Fickian diffusion
KCC-NH ₂ -Quer		7.5	1.480	0.931	0.475	non-Fickian or anomalous diffusion
GSH						
MCM-NH ₂ -Quer	0.5 mM	0.063	0.934	1.2	zero-order	
KCC-NH ₂ -Quer	0.5 mM	0.274	0.964	0.934	zero-order	
MCM-NH ₂ -Quer	2.5 mM	0.170	0.903	0.868	zero-order	
KCC-NH ₂ -Quer	2.5 mM	2.199	0.971	0.371	Fickian diffusion	
MCM-NH ₂ -Quer	10 mM	0.324	0.939	0.680	non-Fickian or anomalous diffusion	
KCC-NH ₂ -Quer	10 mM	1.893	0.974	0.409	Fickian diffusion	

K: rate constant, R: correlation coefficient, n: release exponent.

Table 3: The Korsmeyer-Peppas model fits of quercetin release from two types of MSNs under different pH and GSH conditions.

Table 3. The results indicated that all materials good fit to Korsmeyer-Peppas model, since all R² values were in the range from 0.90 to 0.974. In experiments under pH conditions, the obtained n were: 0.572, 0.548, 0.520, 0.340, 0.243 and 0.475 for MCM-NH₂-Quer (pH 2.5), KCC-NH₂-Quer (pH 2.5), MCM-NH₂-Quer (pH 5), KCC-NH₂-Quer (pH 5), MCM-NH₂-Quer (pH 7.5) and KCC-NH₂-Quer (pH 7.5), respectively.

These results indicate that the Quer release mechanism from this system under pH conditions follows non-Fickian or anomalous diffusion for most samples except KCC-NH₂-Quer (pH 5) and MCM-NH₂-Quer (pH 7.5) follows Fickian diffusion. For instances, MCM-NH₂-Quer (pH 2.5) follows non-Fickian, but this material follows Fickian diffusion at pH 7.5; KCC-NH₂-Quer (pH 5) follows Fickian diffusion, but non-Fickian diffusion at 7.5. This observation, demonstrates that the Quer release mechanism from this system depends on pH value and silica type.

Experiments done under GSH concentrations, the obtained n were: 1.20, 0.934, 0.868, 0.262, 0.680 and 0.409 for MCM-NH₂-Quer (GSH: 0.5 mM), KCC-NH₂-Quer (GSH: 0.5 mM), MCM-NH₂-Quer (GSH: 2.5 mM), KCC-NH₂-Quer (GSH: 2.5 mM), MCM-NH₂-Quer (GSH: 10 mM) and KCC-NH₂-Quer (GSH: 10 mM), respectively. Thus, these results indicate that the Quer release mechanism from this system under GSH conditions follows different mechanisms; most of samples follow zero-order mechanism, while some they follow Fickian and non-Fickian or anomalous diffusion. This observation also indicates that the Quer release mechanism from this system depends on GSH value and silica type. For instances, MCM-NH₂-Quer (GSH: 2.5 mM) follows zero-order mechanism, but follows non-Fickian diffusion with GSH 10 mM; as well as, KCC-NH₂-Quer (GSH: 2.5 and 10) follows Fickian diffusion. This could be due to the described above fact that both of silica types exhibit different morphology structures. The differences in physicochemical properties such the surface area and porosity determine the drug release mechanism via influence the accessibility and mobility of drug molecules inside the pores of silica material and then their release behavior [78,89]. Finally, it can be concluded that the release kinetics of quercetin from our delivery systems depends on stimuli- release condition (pH and GSH) and silica type nanoparticles.

Taken all together, it can be summarized, that this kind of release system shows long-term release, therefore it could be beneficial in biomedical applications. For instance in cancer therapy, because of

acidic tumor environment with pH ~6.8 [90], additionally, due to glutathione acting as trigger release, and its function as an ubiquitous molecule found in the biological system [40], namely the GSH is secreted by tumor cells [91].

Conclusions

The MCM-NH₂-Quer (2D arrangement of pores) and KCC-NH₂-Quer (3D arrangement of pores) MSNs, functionalized with amine-groups and loaded with natural pro-drug quercetin were investigated as a DDSs. Materials characterization indicated that the quantity of Quer present in silica mesopores was higher in case of 2D MSNs (29.11%) than in 3D (26.49%). However, KCC-NH₂-Quer showed importantly better Quer release efficiency (21.3%) than MCM-NH₂-Quer (16.9%). This can be attributed to the unique morphological parameters of KCC-NH₂-Quer such as: fibrous structure with dendrimeric mesopores, arranged in the three-dimensional structure, with wide pore size distribution. Therefore, our results are in agreement with opinion, that structural properties of MSNs carriers play major role in enhancing dissolution of poorly-water soluble quercetin. Moreover, Quer loaded into silica mesopores was in an non-crystalline state in both types of nanoparticles. Thereby, one can expect an improve of drug solubility.

Presented study has also demonstrated that the release of quercetin is pH-glutathione-dependent. Decrease of pH values (more acid environment) and increase of GHS concentrations caused decrease of drug release efficiency. However, in any analogous experimental conditions (pH and glutathione amount) release of quercetin was more intense in case of KCC-NH₂-Quer particles. The maximum value of cumulative release (21.34%) was obtained for KCC-NH₂-Quer and glutathione concentration of 0.5 mM (measured pH value equal to 6.84).

In summary, our results suggest that this simple pH/glutathione-triggers release delivery system of quercetin could be beneficial for long-term release, when could apply in the cancer therapy. In special regards to the silica material type, we believed that the KCC-1 nanoparticles are promising in biomedical applications, especially in controlled DDSs.

Acknowledgement

This work was supported by the National Research Centre (NRC), Egypt. We thank also the Laboratory of Nanostructures for Photonic and Nanomedicine, Institute of High Pressure Physics, Polish Academy of Sciences, Poland. As well as, thanks to The Academy of Scientific Research and Technology, Egypt for the Scientific Exchange.

References

1. Merisko-Liversidge EM, Liversidge GG (2008) Drug nanoparticles: formulating poorly water-soluble compounds. *Toxicol Pathol* 36: 43-48.
2. Hörter D, Dressman JB (2001) Influence of physicochemical properties on dissolution of drugs in the gastrointestinal tract. *Adv Drug Deliv Rev* 46: 75-87.
3. Kesisoglou F, Panmai S, Wu Y (2007) Nanosizing—oral formulation development and biopharmaceutical evaluation. *Adv Drug Deliv Rev* 59: 631-644.
4. Jambhrunkar S, Yu M, Yang J, Zhang J, Shrotri A, et al. (2013) Stepwise pore size reduction of ordered nanoporous silica materials at angstrom precision. *J Am Chem Soc* 135: 8444-8447.
5. Vasconcelos T, Sarmento B, Costa P (2007) Solid dispersions as strategy to improve oral bioavailability of poor water soluble drugs. *Drug Discov Today* 12: 1068-1075.
6. Ambrogi V, Perioli L, Marmottini F, Giovagnoli S, Esposito M, et al. (2007) Improvement of dissolution rate of piroxicam by inclusion into MCM-41 mesoporous silicate. *Eur J Pharm Sci* 32: 216-222.
7. Jambhrunkar S, Qu Z, Popat A, Karmakar S, Xu C, et al. (2014) Modulating in vitro release and solubility of griseofulvin using functionalized mesoporous silica nanoparticles. *J Colloid Interface Sci* 343: 218-225.
8. Mellaerts R, Mols R, Jammaer JA, Aerts CA, Annaert P, et al. (2008) Increasing the oral bioavailability of the poorly water soluble drug itraconazole with ordered mesoporous silica. *Eur J Pharm Biopharm* 69: 223-230.
9. Riikonen J, Correia A, Kovalainen M, Nakkki S, Lehtonen M, et al. (2015) Systematic in vitro and in vivo study on porous silicon to improve the oral bioavailability of celecoxib. *Biomaterials* 52: 44-55.
10. Wu C, Sun X, Zhao Z, Zhao Y, Hao Y, et al. (2014) Synthesis of novel core-shell structured dual-mesoporous silica nanospheres and their application for enhancing the dissolution rate of poorly water-soluble drugs. *Mater Sci Eng C Mater Biol Appl* 44: 262-267.
11. Vallet-Regí M, Rámila A, del Real RP, Pérez-Pariente J (2001) A New Property of MCM-41? Drug Delivery System. *Chemistry of Materials* 13: 308-311.
12. Natarajan SK, Selvaraj S (2014) Mesoporous silica nanoparticles: importance of surface modifications and its role in drug delivery. *RSC Advances* 4: 14328-14334.
13. Vallet-Regí M, Balas F, Arcos D (2007) Mesoporous materials for drug delivery. *Angew Chem Int Ed Engl* 46: 7548-7558.
14. Zhang Y, Zhi Z, Jiang T, Zhang J, Wang Z, et al. (2010) Spherical mesoporous silica nanoparticles for loading and release of the poorly water-soluble drug telmisartan. *J Control Release* 145: 257-263.
15. Kaushal AM, Gupta P, Bansal AK (2004) Amorphous drug delivery systems: molecular aspects, design, and performance. *Crit Rev Ther Drug Carrier Syst* 21: 133-193.
16. Horcajada P, Rámila A, Pérez-Pariente J, Vallet R, Amp, et al. (2004) Influence of pore size of MCM-41 matrices on drug delivery rate. *Microporous and Mesoporous Materials* 68: 105-109.
17. Thomas MJ, Slipper I, Walunj A, Jain A, Favretto ME, et al. (2010) Inclusion of poorly soluble drugs in highly ordered mesoporous silica nanoparticles. *Int J Pharm* 387: 272-277.
18. Li-Hong W, Xin C, Hui X, Li-Li Z, Jing H, et al. (2013) A novel strategy to design sustained-release poorly water-soluble drug mesoporous silica microparticles based on supercritical fluid technique. *Int J Pharm* 454: 135-142.
19. Lamson DW, Brignall MS (2000) Antioxidants and cancer, part 3: quercetin. *Altern Med Rev* 5: 196-208.
20. Choi HJ, Song JH, Park KS, Kwon DH (2009) Inhibitory effects of quercetin 3-rhamnoside on influenza A virus replication. *Eur J Pharm Sci* 37: 329-333.
21. Torres-Piedra M, Ortiz-Andrade R, Villalobos-Molina R, Singh N, Medina-Franco JL, et al. (2010) A comparative study of flavonoid analogues on streptozotocin-nicotinamide induced diabetic rats: Quercetin as a potential antidiabetic agent acting via 11β-Hydroxysteroid dehydrogenase type 1 inhibition. *European Journal of Medicinal Chemistry* 45: 2606-2612.
22. Rotelli AE, Guardia T, Juárez AO, de la Rocha NE, Pelzer LE (2003) Comparative study of flavonoids in experimental models of inflammation. *Pharmacol Res* 48: 601-606.
23. Kumar B, Gupta SK, Nag TC, Srivastava S, Saxena R, et al. (2014) Retinal neuroprotective effects of quercetin in streptozotocin-induced diabetic rats. *Exp Eye Res* 125: 193-202.
24. Hu XT, Ding C, Zhou N, Xu C (2015) Quercetin protects gastric epithelial cell from oxidative damage in vitro and in vivo. *Eur J Pharmacol* 754: 115-124.
25. Egerl S, Wolffram S, Bosy-Westphal A, Boesch-Saadatmandi C, Wagner AE, et al. (2008) Daily quercetin supplementation dose-dependently increases plasma quercetin concentrations in healthy humans. *J Nutr* 138: 1615-1621.
26. Thangasamy T, Sittadjody S, Burd R (2009) Quercetin: A Potential Complementary and Alternative Cancer Therapy. In: Watson RR editor. *Complementary and Alternative Therapies and the Aging Population*. San Diego: Academic Press 563-584.
27. Novo MC, Osugui L, dos Reis VO, Longo-Maugéri IM, Mariano M, et al. (2015) Blockage of Wnt/ β -catenin signaling by quercetin reduces survival and proliferation of B-1 cells in vitro. *Immunobiology* 220: 60-67.
28. Sharmila G, Bhat FA, Arunkumar R, Elumalai P, Raja Singh P, et al. (2014) Chemopreventive effect of quercetin, a natural dietary flavonoid on prostate cancer in *in vivo* model. *Clin Nutr* 33: 718-726.
29. Gugler R, Leschik M, Dengler HJ (1975) Disposition of quercetin in man after single oral and intravenous doses. *Eur J Clin Pharmacol* 9: 229-234.
30. Murakami A, Ashida H, Terao J (2008) Multitargeted cancer prevention by quercetin. *Cancer Lett* 269: 315-325.
31. Cai X, Fang Z, Dou J, Yu A, Zhai G (2013) Bioavailability of quercetin: problems and promises. *Curr Med Chem* 20: 2572-2582.
32. Volate SR, Davenport DM, Muga SJ, Wargovich MJ (2005) Modulation of aberrant crypt foci and apoptosis by dietary herbal supplements (quercetin, curcumin, silymarin, ginseng and rutin). *Carcinogenesis* 26: 1450-1456.
33. Graf BA, Ameho C, Dolnikowski GG, Milbury PE, Chen CY, et al. (2006) Rat gastrointestinal tissues metabolize quercetin. *J Nutr* 136: 39-44.
34. Morand C, Crespy V, Manach C, Besson C, Demigné C, et al. (1998) Plasma metabolites of quercetin and their antioxidant properties. *Am J Physiol* 275: R212-219.
35. Bharali DJ, Siddiqui IA, Adhami VM, Chamcheu JC, Aldahmash AM, et al. (2011) Nanoparticle delivery of natural products in the prevention and treatment of cancers: current status and future prospects. *Cancers (Basel)* 3: 4024-4045.
36. Oussoren C, Storm G (2001) Liposomes to target the lymphatics by subcutaneous administration. *Adv Drug Deliv Rev* 50: 143-156.
37. Berlier G, Gastaldi L, Ugazio E, Miletto I, Iliade P, et al. (2013) Stabilization of quercetin flavonoid in MCM-41 mesoporous silica: positive effect of surface functionalization. *J Colloid Interface Sci* 393: 109-118.
38. Li ZJ, Zhang YJ, Zhang HW, Fu HX (2013) Long-lasting phosphorescence functionalization of mesoporous silica nanospheres by CaTiO₃:Pr³⁺ for drug delivery. *Microporous and Mesoporous Materials* 176: 48-54.
39. Sapino S, Ugazio E, Gastaldi L, Miletto I, Berlier G, et al. (2015) Mesoporous silica as topical nanocarriers for quercetin: characterization and *in vitro* studies. *Eur J Pharm Biopharm* 89: 116-125.
40. Huang X, Zhang T, Goswami A, Luo F, Asefa T (2015) Glutathione-triggered release of model drug molecules from mesoporous silica nanoparticles via a non-redox process. *RSC Advances* 5: 28836-28839.
41. Lu J, Li Z, Zink JI, Tamanoi F (2012) In vivo tumor suppression efficacy of mesoporous silica nanoparticles-based drug-delivery system: enhanced efficacy by folate modification. *Nanomedicine: Nanotechnology, Biology and Medicine* 8: 212-220.
42. Polshettiwar V, Cha D, Zhang X, Basset JM (2010) High-surface-area silica nanospheres (KCC-1) with a fibrous morphology. *Angew Chem Int Ed Engl* 49: 9652-9656.
43. Moon DS, Lee JK (2012) Tunable synthesis of hierarchical mesoporous silica nanoparticles with radial wrinkle structure. *Langmuir* 28: 12341-12347.
44. Huang X, Tao Z, Praskavich JC Jr, Goswami A, Al-Sharab JF, et al. (2014) Dendritic silica nanomaterials (KCC-1) with fibrous pore structure possess high DNA adsorption capacity and effectively deliver genes *in vitro*. *Langmuir* 30: 10886-10898.
45. Limnell T, Santos HA, Mäkilä E, Heikkilä T, Salonen J, et al. (2011) Drug delivery

- formulations of ordered and nonordered mesoporous silica: comparison of three drug loading methods. *J Pharm Sci* 100: 3294-3306.
46. Jambhrunkar S, Karmakar S, Popat A, Yu M, Yu C (2014) Mesoporous silica nanoparticles enhance the cytotoxicity of curcumin. *RSC Advances* 4: 709-712.
47. Mani G, Pushparaj H, Peng MM, Muthiahpillai P, Udhumannsha U, et al. (2014) Synthesis and characterization of pharmaceutical surfactant templated mesoporous silica: Its application to controlled delivery of duloxetine. *Materials Research Bulletin* 51: 228-235.
48. Zhu W, Wan L, Zhang C, Gao Y, Zheng X, et al. (2014) Exploitation of 3D face-centered cubic mesoporous silica as a carrier for a poorly water soluble drug: influence of pore size on release rate. *Mater Sci Eng C Mater Biol Appl* 34: 78-85.
49. Horcajada P, Rámila A, Férey G, Vallet-Regí M (2006) Influence of superficial organic modification of MCM-41 matrices on drug delivery rate. *Solid State Sciences* 8: 1243-1249.
50. Jambhrunkar S, Qu Z, Popat A, Yang J, Noonan O, et al. (2014) Effect of surface functionality of silica nanoparticles on cellular uptake and cytotoxicity. *Mol Pharm* 11: 3642-3655.
51. Vialpando M, Aerts A, Persoons J, Martens J, Van Den Mooter G (2011) Evaluation of ordered mesoporous silica as a carrier for poorly soluble drugs: influence of pressure on the structure and drug release. *J Pharm Sci* 100: 3411-3420.
52. Halamová D, Badaniová M, Zelenák V, Gondová T, Vainio U (2010) Naproxen drug delivery using periodic mesoporous silica SBA-15. *Applied Surface Science* 256: 6489-6494.
53. Datt A, El-Maazawi I, Larsen SC (2012) Aspirin Loading and Release from MCM-41 Functionalized with Aminopropyl Groups via Co-condensation or Postsynthesis Modification Methods. *The Journal of Physical Chemistry C* 116: 18358-18366.
54. Guo Z, Liu XM, Ma L, Li J, Zhang H, et al. (2013) Effects of particle morphology, pore size and surface coating of mesoporous silica on Naproxen dissolution rate enhancement. *Colloids Surf B Biointerfaces* 101: 228-235.
55. Gayam SR, Wu S-P (2014) Redox responsive Pd(ii) templated rotaxane nanovalve capped mesoporous silica nanoparticles: a folic acid mediated biocompatible cancer-targeted drug delivery system. *Journal of Materials Chemistry B* 2: 7009-7016.
56. Kim J, Seidler P, Wan LS, Fill C (2009) Formation, structure, and reactivity of amino-terminated organic films on silicon substrates. *J Colloid Interface Sci* 329: 114-119.
57. Li Z, Su K, Cheng B, Deng Y (2010) Organically modified MCM-type material preparation and its usage in controlled amoxicillin delivery. *J Colloid Interface Sci* 342: 607-613.
58. Song SW, Hidajat K, Kawi S (2005) Functionalized SBA-15 materials as carriers for controlled drug delivery: influence of surface properties on matrix-drug interactions. *Langmuir* 21: 9568-9575.
59. Kim J, Seidler P, Fill C, Wan LS (2008) Investigations of the effect of curing conditions on the structure and stability of amino-functionalized organic films on silicon substrates by Fourier transform infrared spectroscopy, ellipsometry, and fluorescence microscopy. *Surface Science* 602: 3323-3330.
60. Mäkilä E, Bimbo LM, Kaasalainen M, Herranz B, Airaksinen AJ, et al. (2012) Amine modification of thermally carbonized porous silicon with silane coupling chemistry. *Langmuir* 28: 14045-14054.
61. Andrade GF, Soares DCF, Almeida RKdS, Sousa E (2012) Mesoporous Silica SBA-16 Functionalized with Alkoxy silane Groups: Preparation, Characterization, and Release Profile Study. *Journal of Nanomaterials* 2012: 10.
62. Chung TH, Wu SH, Yao M, Lu CW, Lin YS, et al. (2007) The effect of surface charge on the uptake and biological function of mesoporous silica nanoparticles in 3T3-L1 cells and human mesenchymal stem cells. *Biomaterials* 28: 2959-2966.
63. Lee CH, Lo LW, Mou CY, Yang CS (2008) Synthesis and Characterization of Positive-Charge Functionalized Mesoporous Silica Nanoparticles for Oral Drug Delivery of an Anti-Inflammatory Drug. *Advanced Functional Materials* 18: 3283-3292.
64. Lvov Y, Ariga K, Onda M, Ichinose I, Kunitake T (1997) Alternate Assembly of Ordered Multilayers of SiO₂ and Other Nanoparticles and Polyions. *Langmuir* 13: 6195-6203.
65. Hu L, Sun C, Song A, Chang D, Zheng X, et al. (2014) Alginate encapsulated mesoporous silica nanospheres as a sustained drug delivery system for the poorly water-soluble drug indomethacin. *Asian Journal of Pharmaceutical Sciences* 9: 183-190.
66. Popat A, Jambhrunkar S, Zhang J, Yang J, Zhang H, et al. (2014) Programmable drug release using bioresponsive mesoporous silica nanoparticles for site-specific oral drug delivery. *Chem Commun (Camb)* 50: 5547-5550.
67. Marcilla A, Gómez A, Menargues S (2005) TGA/FTIR study of the evolution of the gases evolved in the catalytic pyrolysis of ethylene-vinyl acetate copolymers. Comparison among different catalysts. *Polymer Degradation and Stability* 89: 454-460.
68. Schindler A, Neumann G, Rager A, Füglein E, Blumm J, et al. (2013) A novel direct coupling of simultaneous thermal analysis (STA) and Fourier transform-infrared (FT-IR) spectroscopy. *Journal of Thermal Analysis and Calorimetry* 113: 1091-1102.
69. Vunain E, Opembe N, Jalama K, Mishra A, Meijboom R (2014) Thermal stability of amine-functionalized MCM-41 in different atmospheres. *Journal of Thermal Analysis and Calorimetry* 115: 1487-1496.
70. Parida KM, Rath D (2009) Amine functionalized MCM-41: An active and reusable catalyst for Knovenagel condensation reaction. *Journal of Molecular Catalysis A: Chemical* 310: 93-100.
71. Qu F, Zhu G, Huang S, Li S, Sun J, et al. (2006) Controlled release of Captopril by regulating the pore size and morphology of ordered mesoporous silica. *Microporous and Mesoporous Materials* 92: 1-9.
72. Cauda V, Mühlstein L, Onida B, Bein T (2009) Tuning drug uptake and release rates through different morphologies and pore diameters of confined mesoporous silica. *Microporous and Mesoporous Materials* 118: 435-442.
73. Jal PK, Patel S, Mishra BK (2004) Chemical modification of silica surface by immobilization of functional groups for extractive concentration of metal ions. *Talanta* 62: 1005-1028.
74. Xu Y, Wang C, Zhou G, Wu Y, Chen J (2012) Improving the controlled release of water-insoluble emodin from amino-functionalized mesoporous silica. *Applied Surface Science* 258: 6366-6372.
75. Costa P, Sousa Lobo JM (2001) Modeling and comparison of dissolution profiles. *Eur J Pharm Sci* 13: 123-133.
76. Aznar E, Sancenón F, Marcos MD, Martínez-Máñez R, Stroeve P, et al. (2012) Delivery modulation in silica mesoporous supports via alkyl chain pore outlet decoration. *Langmuir* 28: 2986-2996.
77. Nadrah P, Maver U, Jemec A, Tišler T, Bele M, et al. (2013) Hindered Disulfide Bonds to Regulate Release Rate of Model Drug from Mesoporous Silica. *ACS Applied Materials & Interfaces* 5: 3908-3915.
78. Nieto A, Colilla M, Balas F, Vallet-Regí M (2010) Surface electrochemistry of mesoporous silicas as a key factor in the design of tailored delivery devices. *Langmuir* 26: 5038-5049.
79. Gao L, Sun J, Zhang L, Li Y, Ren B (2011) Thermal decomposition behavior of amino groups modified bimodal mesoporous silicas as aspirin carrier. *J Nanosci Nanotechnol* 11: 10324-10332.
80. Popovici RF, Seftel EM, Mihai GD, Popovici E, Voicu VA (2011) Controlled drug delivery system based on ordered mesoporous silica matrices of captopril as angiotensin-converting enzyme inhibitor drug. *J Pharm Sci* 100: 704-714.
81. Zhu YF, Shi JL, Li YS, Chen HR, Shen WH, et al. (2005) Storage and release of ibuprofen drug molecules in hollow mesoporous silica spheres with modified pore surface. *Microporous and Mesoporous Materials* 85: 75-81.
82. Carriazo D, del Arco M, Fernández A, Martín C, Rives V (2010) Inclusion and release of fenbufen in mesoporous silica. *J Pharm Sci* 99: 3372-3380.
83. Zhang Y, Huo M, Zhou J, Zou A, Li W, et al. (2010) DDSolver: an add-in program for modeling and comparison of drug dissolution profiles. *AAPS J* 12: 263-271.
84. Slowing II, Vivero-Escoto JL, Wu CW, Lin VS (2008) Mesoporous silica nanoparticles as controlled release drug delivery and gene transfection carriers. *Adv Drug Deliv Rev* 60: 1278-1288.
85. Lin CX, Qiao SZ, Yu CZ, Ismadji S, Lu GQ (2009) Periodic mesoporous silica and organosilica with controlled morphologies as carriers for drug release. *Microporous and Mesoporous Materials* 117: 213-219.
86. Korsmeyer RW, Gurny R, Doelker E, Buri P, Peppas NA (1983) Mechanisms

- of solute release from porous hydrophilic polymers. *International Journal of Pharmaceutics* 15: 25-35.
87. Ritger PL, Peppas NA (1987) A simple equation for description of solute release I. Fickian and non-fickian release from non-swellable devices in the form of slabs, spheres, cylinders or discs. *Journal of Controlled Release* 5: 23-36.
88. Peppas NA (1985) Analysis of Fickian and non-Fickian drug release from polymers. *Pharm Acta Helv* 60: 110-111.
89. Ukmar T, Maver U, Planinšek O, Kaučič V, Gaberšček M, et al. (2011) Understanding controlled drug release from mesoporous silicates: theory and experiment. *J Control Release* 155: 409-417.
90. Colilla M, Gonzalez B, Vallet-Regi M (2013) Mesoporous silica nanoparticles for the design of smart delivery nanodevices. *Biomaterials Science* 1: 114-134.
91. Liu R, Zhao X, Wu T, Feng P (2008) Tunable redox-responsive hybrid nanogated ensembles. *J Am Chem Soc* 130: 14418-14419.